energy&fuels

Open Access

pubs.acs.org/EF

Article

Properties of ZrO_2:3 mol % Y_2O_3−$(Na,K)_2CO_3$−$(Li,Na,K)_2CO_3$ Triple-Layer Membranes for Carbon Dioxide Ion Permeation

Tatiane C. Porfirio, Eliana N. S. Muccillo, and Reginaldo Muccillo*

Cite This: *Energy Fuels* 2024, 38, 9890−9897

Read Online

ACCESS | Metrics & More | Article Recommendations

ABSTRACT: ZrO_2:3 mol % Y_2O_3 (3YSZ) ceramic powders were thoroughly mixed with poly(methyl methacrylate) (PMMA), pressed into pellets, and subjected to heat treatment to prepare porous ceramics with high skeletal density by thermally removing PMMA. The porous 3YSZ pellets were first impregnated with a molten eutectic $(Na,K)_2CO_3$ (NKC) composition at 710 °C, followed by cooling to 420 °C for impregnation with a molten eutectic $(Li,Na,K)_2CO_3$ (LNKC) composition. The presence of sodium and potassium was evaluated by performing energy-dispersive X-ray analyses on the surfaces of triple-layer membranes. Permeation measurements were performed by using a homemade gas permeation setup. Electrical conductivity of carbon dioxide ions across the pellet thickness was measured at 475 °C for over 200 h by using impedance spectroscopy. No significant degradation of the electrical conductivity profile was observed during the test period, suggesting that the solid NKC layer acted as a protective barrier, preventing interaction between the 3YSZ ceramic and molten LNKC within the pore network.

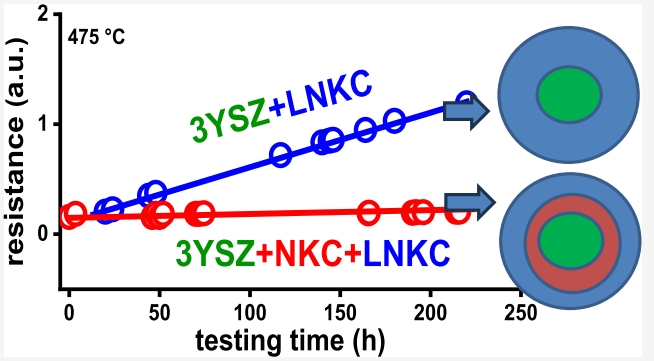

1. INTRODUCTION

In recent decades, the global demand for energy has reached unprecedented levels due to the ever-increasing needs of humanity. Critical environmental concerns, with issues such as the greenhouse effect, carbon dioxide emissions, global warming, and climate change, have stimulated several studies. Carbon dioxide (CO_2) is a key player in the greenhouse effect, and its accumulation in the Earth's atmosphere stands as a primary driver of global warming. CO_2 accumulation in the atmosphere is one of the main causes of global warming due to a range of human activities, including fuel burning, deforestation, cement manufacturing, livestock farming, and fertilization. These activities contribute to increasing the concentration of CO_2 in the atmosphere, resulting in an increase in Earth's temperature.

Carbon dioxide capture, utilization, and storage refers to the technologies that remove CO_2 directly from the atmosphere, preventing its accumulation. One of the investigated solutions in recent years, collaborating to minimize the harmful effects of polluting gases in the atmosphere, is the capture of CO_2 by ionic conducting composite dual-phase inorganic membranes.[1−10] Those composites consist of porous solid electrolytes already in use in solid oxide fuel cells, impregnated with alkali metal carbonates.[8] Their average pore size must be larger than the dimensions of the mobile gaseous species. The solid phase, an oxygen ion conductor, is the support for a molten eutectic composition of alkaline carbonates and a carbon dioxide ion conductor, leading to composite membranes able to permeate CO_2.[11−14] This ability is due to their improved selectivity and permeability as well as chemical and physical stability. Moreover, they have significant ion conductivity due to the nature of their constituent phases.[15−18] The total efficiency depends on the ionic conductivity of both solid and liquid phases, the eutectic composition, and the overall conductivity of the membrane.[19] During operation of the dual membrane, the species to be permeated, namely, the carbon dioxide ions, diffuses through the pores of the solid matrix due to concentration gradients between the feed and the permeated sides of the membrane. Oxygen is permeated by ionic conduction through the O^{2-} ion vacancies of the crystalline structure with high mobility at the melting point of the infiltrated carbonates. The oxygen incorporation reaction occurs close to the membrane surface, diffusing the ions through the bulk of the ceramic. Ionic transport also happens in the permeation of CO_2 through molten carbonates as CO_3^{2-} ions, differing from the case of oxides due to the fact that the

Received: December 29, 2023
Revised: May 5, 2024
Accepted: May 13, 2024
Published: May 21, 2024

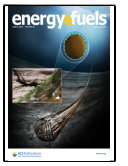

liquid is amorphous. The carbonate ion transport occurs by diffusion in the liquid due to an electrochemical potential gradient. The CO_2 capture/separation is then entirely based on ionic transport through the condensed phases, and gas phase diffusion must be avoided by using physically impermeable membranes.[20]

One of the challenges regarding the use of molten carbonates in a ceramic matrix concerns the stability of the phases. Ionic conductors, such as those based on zirconia, showed reactions with molten salts,[6] which could promote degradation of the membrane during operation. In addition, membranes can experience degradation due to the interaction/deposition of the membrane surface with encrustations[21] besides salts, such as colloids, macromolecules, among others, in which, by reacting physically and chemically with the membrane interfaces, can temporarily or permanently reduce the composite operation by the surface absorption or even pore blockage.[22] Thus, the preparation of a protective layer becomes an interesting point to prolong the useful life of the composite membranes.

In this work, porous ZrO_2:3 mol % Y_2O_3 (3YSZ) was used as a matrix due to its mechanical properties and chemical stability, which are important properties in materials used in membranes.[23] The insertion of a protective layer composed of a eutectic composition of sodium and potassium carbonates (Na_2CO_3–K_2CO_3, NKC) is tested in the composite membrane. Figure 1 shows a sketch of the proposed membrane

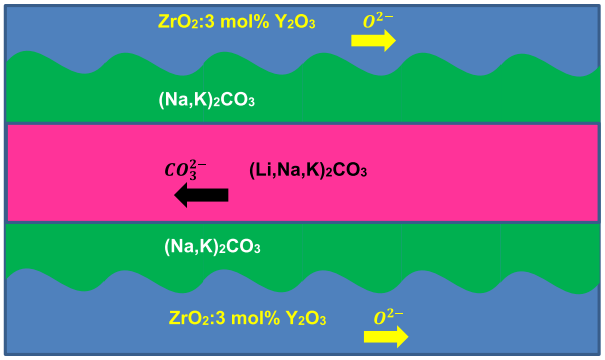

Figure 1. Schematic illustration of a ceramic-carbonate triple-phase membrane for CO_2 separation: 3YSZ porous matrix impregnated with a $(Na,K)_2CO_3$ layer and afterward with $(Li,Na,K)_2CO_3$.

for operation at the melting point of LNKC, with the oxygen ion conducting 3YSZ, the nonconducting NKC, and the carbon dioxide ion conducting LNKC.

The purpose was to improve the permeation process, avoiding the interaction between the ceramic matrix and the molten carbonates. The effectiveness of this approach was ascertained with long endurance tests, collecting ionic conductivity data at the operating temperature of the membrane.

2. MATERIALS AND METHODS

2.1. Ceramic Membranes. 3YSZ (Tosoh Corporation, Japan) ceramic powders, poly(methyl methacrylate) (PMMA, Tokyo Chemical Industry, Japan), lithium carbonate (Li_2CO_3 99.9%, Synth, Brazil), sodium carbonate (Na_2CO_3 99.5%. ECIBRA, Brazil), and potassium carbonate (K_2CO_3 99.9%, Sigma-Aldrich, Spain) were used. Composite ceramic membranes were prepared by infiltrating the eutectic compositions of the molten carbonates into porous 3YSZ pellets. To obtain the porous ceramic, 3YSZ and 50 vol % PMMA were ball-milled in ethanol for 4 h. After drying, the powder was uniaxially pressed at 50 MPa into 10 mm diameter, 2 mm thickness pellets, and heated at 2 °C min^{-1} to 425 °C for 2 h for thermally removing the PMMA, followed by heating at 5 °C min^{-1} to 1400 °C for 2 h for sintering, and cooling at 10 °C min^{-1} to room temperature, to obtain porous 3YSZ with high skeletal density (5.95 g cm^{-1}, 97.5% T.D.).[24] Apparent density and porosity were evaluated by the Archimedes technique in a Mettler Toledo AG245 (Columbus, OH, USA) analytical balance.

Two impregnation processes were required to obtain ceramic membranes with protective layer. The first one, corresponding to the protection layer, was obtained by placing the eutectic composition of NKC (56 mol % Na_2CO_3: 44 mol % K_2CO_3, 710 °C M.P.)[25] on top of the porous 3YSZ matrix surface and heating at 5 °C min^{-1} to 750 °C for 1 h, to allow for the molten carbonate to percolate through the pores. The impregnation occurred by gravity and capillarity forces. After cooling, the pellet was heated to 800 °C for 45 min to partially remove the NKC and ensure that an NKC layer remained inside the ceramic skeleton. The second step involved impregnation of LNKC to obtain the composite membrane. For that purpose, the eutectic composition of LNKC (43.5 mol % Li_2CO_3:31.5 mol % Na_2CO_3: 25 mol % K_2CO_3, 397 °C M.P.)[25] was placed on top of the porous ceramic containing the protective layer and heated at 5 °C min^{-1} to 450 °C for 1 h to allow the molten LNKC to fill up the open pores. Porous 3YSZ pellets impregnated solely with molten LNKC were prepared as well.

2.2. Thermal Analysis. Thermal characterization of the eutectic compositions of the carbonates was carried out by simultaneous thermogravimetry, TG, and differential thermal analysis, DTA (STA 409 E, Netzsch, Selb, Germany); the measurements were performed under flowing synthetic air at 10 L min^{-1}, with a 5 °C min^{-1} heating rate from room temperature to a temperature higher than the melting point of the carbonates. Alpha-alumina was used as reference. Thermal analyses were performed in 3YSZ/NKC and in 3YSZ/LNKC mixtures (both 50:50 wt %) as well, looking for eventual chemical reactions between the solid electrolyte and the carbonates at their melting points.

2.3. Structural Analysis (XRD and SEM). Structural phase analysis was carried out by X-ray diffraction (XRD) measurements at room temperature on pellet surfaces in a D8 Advance diffractometer (Bruker-AXS, Karlsruhe, Germany) with θ–θ Bragg–Brentano configuration, 40 kV-40 mA Ni-filtered Cuk_α radiation (λ = 1.5405 Å), in the $20° \leq 2\theta \leq 80°$ range, 0.05° step size, 5 s per step. The pore distribution was analyzed with scanning electron microscopy (SEM)(Inspect F50 FEG-SEM, FEI, Brno, Czech Republic) at both parallel and fractured pellet surfaces. The impregnation effectiveness was ascertained with an EDX spectrometer (Octane Elect, Ametek, Inc., Mahwah, NJ, USA). EDX data were collected at 20 kV, 6.5 spot size, in parallel pellet surfaces covered with 2-propanol-diluted colloidal graphite (dag dispersion 154, Acheson Colloids Co., Port Huron, MI, USA).

2.4. Electrical Measurements. Impedance spectroscopy measurements were carried out from 5 Hz to 13 MHz, 200 mV input signal, at temperatures in the 350–530 °C range with a Hewlett-Packard 4192A impedance analyzer connected to a HP 362 controller (Yokogawa Hewlett-Packard, Tokyo, Japan). The pellets were spring-loaded to an alumina sample holder, with platinum leads connected to the impedance analyzer.[26] Platinum grids and gold foil electrodes were positioned at both parallel surfaces of the ceramic pellet. The sample holder was inserted into a programmable tubular furnace. The temperature was monitored with a chromel–alumel thermocouple with its tip positioned close to the pellet. Figure 2 shows a sketch describing the experimental setup.

2.5. Permeation Measurements. Permeation measurements were conducted using an experimental setup developed and assembled in our laboratories.[27] The setup comprises an alumina sample holder placed within a three-atmosphere chamber, with carbon dioxide and argon introduced on each side and a third gas, either argon or nitrogen, used to sweep out any eventual leakage. This entire setup is positioned within a programmable furnace. All gases

https://doi.org/10.1021/acs.energyfuels.3c05216
Energy Fuels 2024, 38, 9890–9897

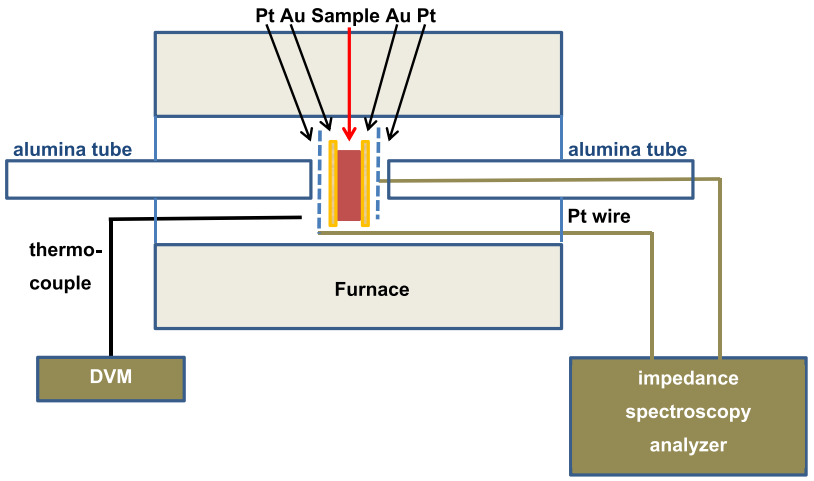

Figure 2. Sketch of the experimental setup for the evaluation of the electrical conductivity of composite ceramic membranes: impedance spectroscopy analyzer: Hewlett-Packard 4192A; DVM: Hewlett-Packard 974A digital voltmeter.

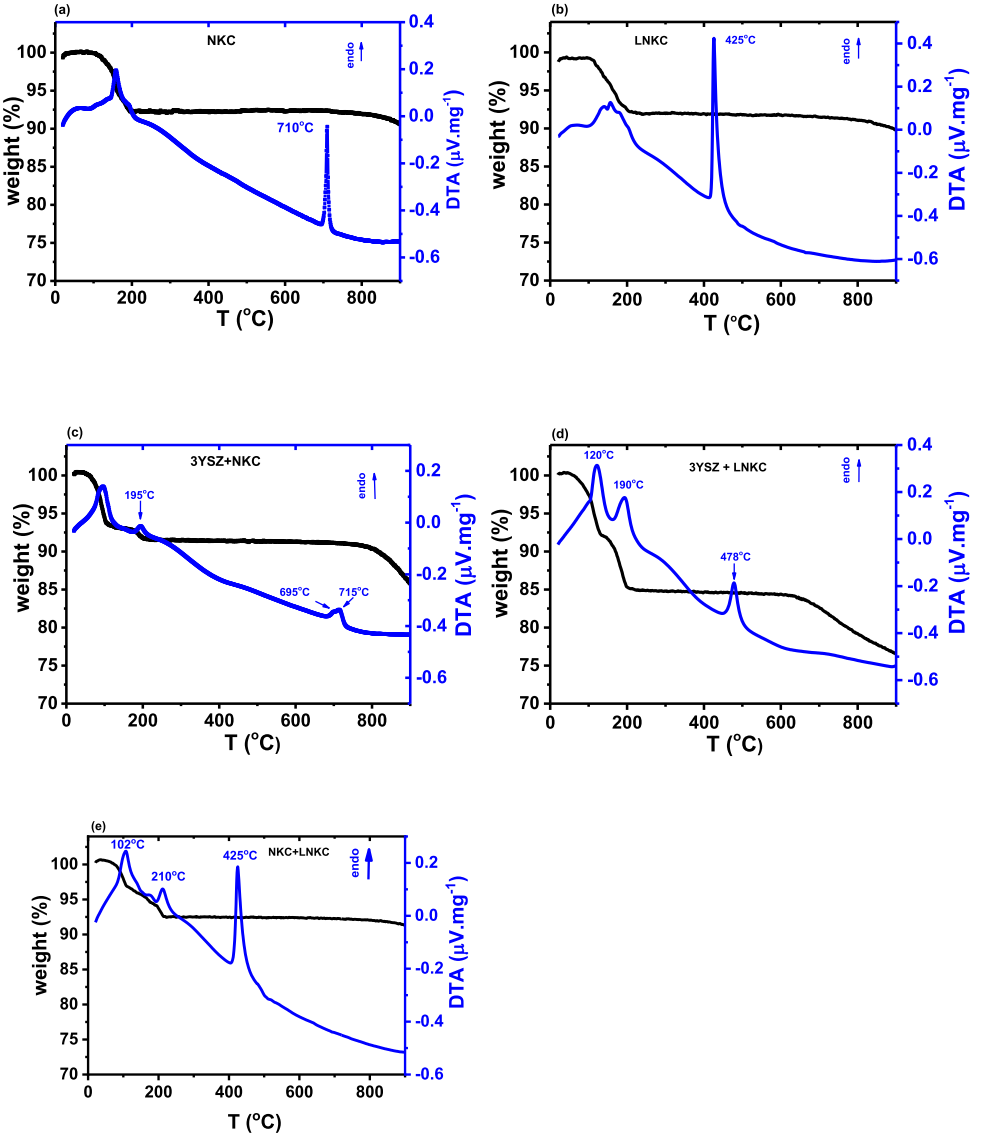

Figure 3. TG and DTA curves of eutectic compositions of (a) $(Na,K)_2CO_3$–NKC, (b) $(Li,Na,K)_2CO_3$–LNKC, (c) 3YSZ + NKC, (d) 3YSZ + LNKC, and (e) NKC + LNKC. The compositions in (c–e) were 50–50 wt %.

https://doi.org/10.1021/acs.energyfuels.3c05216
Energy Fuels 2024, 38, 9890–9897

are provided through mass flow controllers (MKS Instruments, Inc., Methuen, MA, USA) and the flow evaluated with a mass spectrometer (Thermostar, Pfeiffer Vacuum GmbH, Asslar, Germany).[27]

3. RESULTS AND DISCUSSION

3.1. Ceramic Membranes. To obtain porous membranes to be impregnated with molten carbonates, PMMA was added to the 3YSZ powder as a sacrificial pore former to be thermally removed during sintering. Samples with approximately 60% relative density (T.D. = 6.05 g·cm^{-3})[24] with 42% open porosity were obtained.

3.2. Thermal Analysis. Figure 3 shows TG and DTA curves, in the room temperature to 900 °C range, of eutectic compositions of (a) sodium potassium carbonates (NKC), (b) lithium sodium potassium carbonates (LNKC), (c) 3YSZ + NKC (50−50 wt %), (d) 3YSZ + LNKC (50−50 wt %), and (e) NKC + LNKC (50−50 wt %). The weight loss of all compositions became constant at temperatures higher than approximately 200 °C. The weight losses of NKC and LNKC were approximately 7 and 6%, respectively, apparently due to elimination of water and organic compounds. The melting points of NKC and LNKC eutectic compositions were evaluated as 710 and 425 °C for NKC (Figure 3a) and LNKC (Figure 3b), respectively. For NKC + LNKC (Figure 3e), the melting point was also 425 °C, apparently evidence that NKC did not react with LNKC up to the membrane operating temperature (<480 °C), allowing for using NKC as a protective layer to prevent any reaction of LNKC with the 3YSZ matrix. The DTA endothermic peaks near the melting points of NKC and LNKC of 3YSZ + NKC (Figure 3c) and of 3YSZ + LNKC (Figure 3d) are wider than those of pure NKC and LNKC and have two maxima instead of one compared to the DTA curves of NKC and LNKC, respectively, showing that chemical reaction occurred between the solid electrolyte and the alkali salts.

3.3. Structural Analysis (XRD and SEM). The SEM micrographs of the surfaces of porous 3YSZ, porous 3YSZ impregnated with NKC, porous 3YSZ impregnated with LNKC, and porous 3YSZ impregnated with NKC and sequentially with LNKC are shown in Figure 4.

Pores in the micrometer range are evident at the surface of the 3YSZ ceramics after removal of the sacrificial pore former (Figure 4, top left position). The microstructure consists mostly of small grains along with interconnected porosity. A detailed analysis of several regions of the 3YSZ surface showed that pore sizes ranged from 1.3 to 2.0 μm. The high magnification image with focus inside one of the pores of 3YSZ after impregnation of molten NKC (Figure 4, right positions) shows the NKC presence, characterized by rod-shaped structures pointed at by the yellow arrows. The same behavior is observed in porous 3YSZ after impregnation of molten LNKC, also identified by smaller rod-shaped structures, signaled by the yellow arrow. The combined NKC + LNKC impregnation shows the carbonates located at the vicinity of the pores, apparently lining the pore surfaces. Evidence that the carbonates permeate through the pores is obtained by FEG-SEM-EDX analysis of fracture surfaces.

The analysis shows that sodium and potassium were detected at the surfaces of the membranes impregnated with the alkali salts. The detected contents depend on the location of the surface, being more pronounced in the vicinity of the pores.

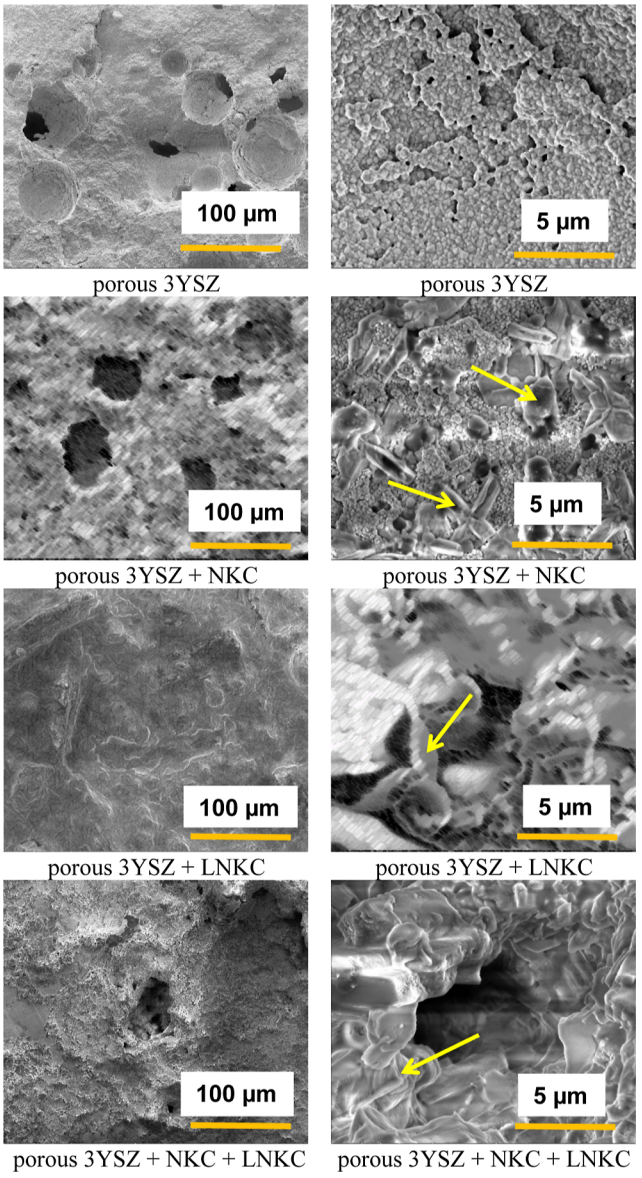

Figure 4. From top to bottom: SEM micrographs of surfaces of porous 3YSZ, porous 3YSZ impregnated with NKC, porous 3YSZ impregnated with LNKC, and porous 3YSZ impregnated with NKC and sequentially with LNKC; right column: figures with higher magnification. The arrows point to the carbonate phase.

The SEM image and EDX spectrum of a fracture surface of 3YSZ impregnated with LNKC are shown in Figure 5. The presence of sodium (lithium is not detected by this technique) is confirmed.

SEM images of the fracture surface of the porous 3YSZ impregnated with the NKC protective layer were observed after long-term endurance tests at 475 °C. The results are shown in Figure 6.

The EDX plot shows that after the long-term test, the carbonate phase is still deposited into the fracture surface of the ceramic membrane. Potassium and sodium elements were detected in the composite, as well as zirconium, yttrium, and oxygen.

The XRD patterns of the polished sintered surface of the porous 3YSZ ceramic matrix before and after impregnation with carbonates are depicted in Figure 7.

https://doi.org/10.1021/acs.energyfuels.3c05216
Energy Fuels 2024, 38, 9890−9897

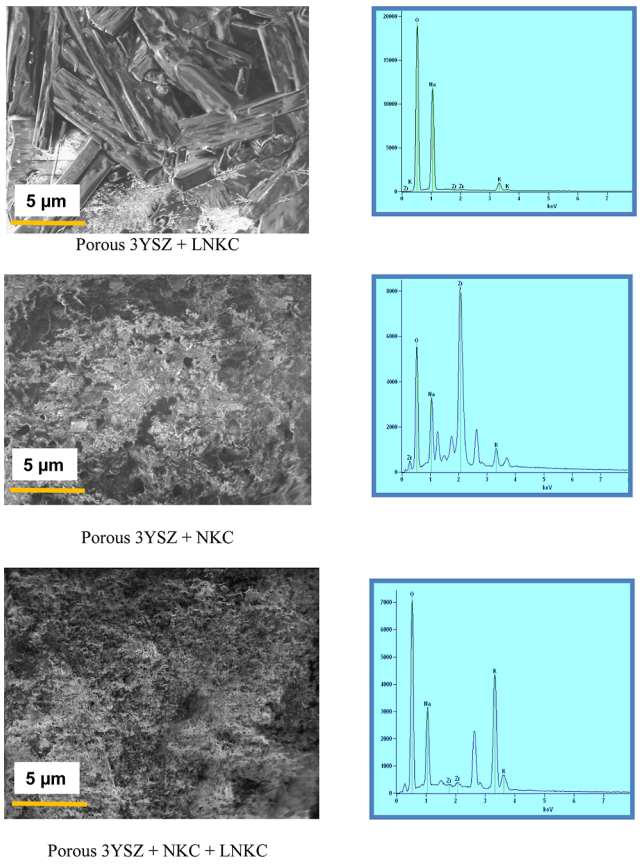

Figure 5. SEM micrographs (left) and EDX diagrams (right) of the fracture surface of porous 3YSZ impregnated with $(Li,Na,K)_2CO_3$, $(Na,K)_2CO_3$, and $(Na,K)_2CO_3$ followed by $(Li,Na,K)_2CO_3$.

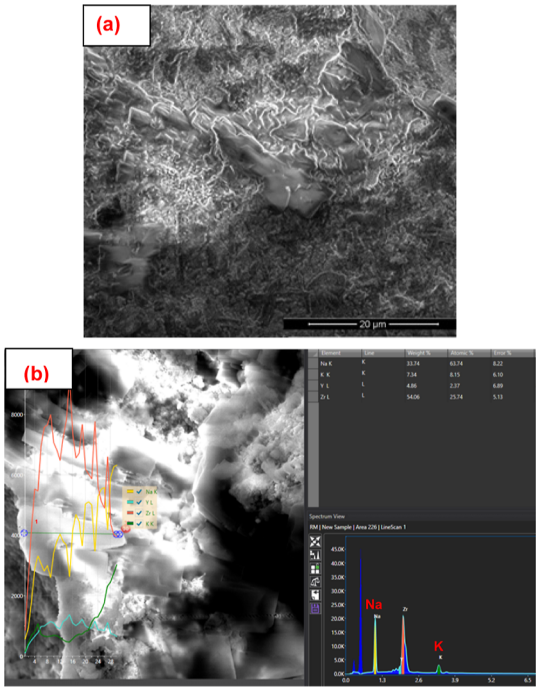

Figure 6. SEM micrographs and EDS diagram of the fracture surface of 3YSZ impregnated with (a) $(Na,K)_2CO_3$ and (b) $(Li,Na,K)_2CO_3$ after long-term endurance tests at 475 °C.

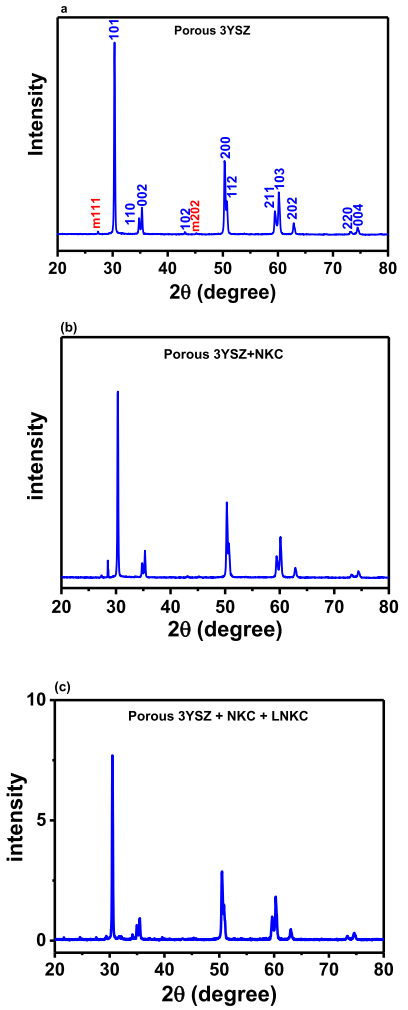

Figure 7. XRD patterns of (a) porous 3YSZ, (b) porous 3YSZ impregnated with $(Na,K)_2CO_3$, and (c) porous 3YSZ impregnated with $(Na,K)_2CO_3$ and $(Li,Na,K)_2CO_3$. Miller indices are in the top figure.

The porous 3YSZ ceramics either pure (Figure 7a) or impregnated with NKC and with NKC + LNKC show the predominant tetragonal phase of 3YSZ with minor traces of the monoclinic phase.[28,29] Polishing the ceramic membranes after impregnation removed extra alkali salts from the surfaces.

3.4. Electrical Measurements. Impedance spectroscopy diagrams collected at several temperatures on porous 3YSZ and 3YSZ impregnated with LNKC and with NKC + LNKC sintered pellets are shown in Figure 8. The $[-Z''(\omega) \times Z'(\omega)]$ impedance diagrams of porous 3YSZ (Figure 8a) is composed of a single semicircle due to contributions of grains (bulk) and interfaces (grain boundaries and mainly pores),[30,31] the total electrical resistivity decreasing for increasing temperature. The impedance diagram of the composite dual membrane of porous 3YSZ impregnated with LNKC (Figure 8b), on the other hand, has apparently two semicircles, with the total electrical resistance decreasing up to the melting point of the eutectic mixture. For higher temperatures, the diagram represents the electrode contribution at frequencies lower than 1 kHz; at higher frequencies, the reactance Z'' extends to positive values due to the inductance of the platinum leads connecting the gold electrodes to the impedance analyzer.[32] Moreover, at temperatures higher than the melting point of the

https://doi.org/10.1021/acs.energyfuels.3c05216
Energy Fuels 2024, 38, 9890−9897

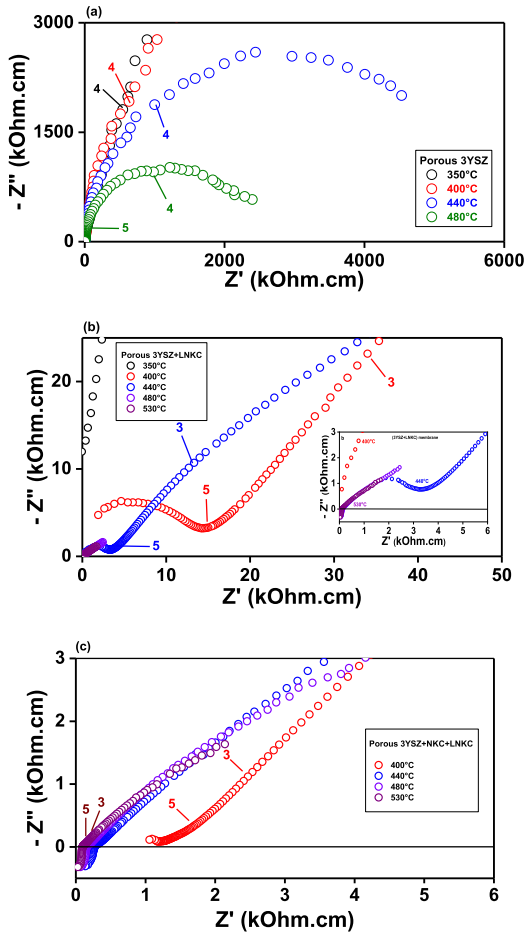

Figure 8. Impedance spectroscopy diagrams of (a) porous 3YSZ, (b) porous 3YSZ impregnated with $(Li,Na,K)_2CO_3$ (with inset for the low resistivity data), and (c) porous 3YSZ impregnated with $(Na,K)_2CO_3$ and $(Li,Na,K)_2CO_3$.

composite ceramic membrane, the carbon dioxide ion electrical conductivity within the molten carbonate predominates, being more than 3 orders of magnitude higher than that of the oxygen ions within the solid electrolyte ceramic phase. This behavior is quite evident in the membrane containing the protective layer (Figure 8c), i.e., at temperatures higher than 440 °C, the electrical conduction of the carbonate ions prevails.

Figure 9 shows the Arrhenius plots of the electrical conductivity of the porous 3YSZ and the alkali-salt-impregnated porous 3YSZ pellets. The activation energy is lower for temperatures higher than the melting point of the carbonates. For temperatures below approximately 400 °C, the predominant mechanism is the conduction of oxygen ions by 3YSZ, with an activation energy value of approximately 1.3 eV, typical of yttria-stabilized zirconia.[33] In the 400−480 °C range, there is an abrupt increase of the ionic conductivity due to the contribution of the conductivity of the molten carbonates, enhancing charge transport. For temperatures higher than 480 °C, ionic conduction occurs preferentially through the molten carbonates.

Figure 10 shows electrical resistance values at 300 kHz, collected in the impedance spectroscopy diagrams of the 3YSZ + NKC + LNKC membrane, maintained at 475 °C for 20−220 h time duration.

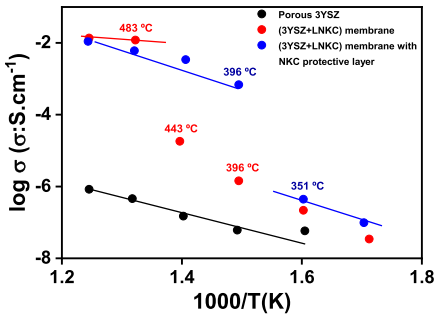

Figure 9. Arrhenius plots of the electrical conductivity of porous 3YSZ, porous 3YSZ impregnated with $(Li,Na,K)_2CO_3$, and porous 3YSZ impregnated with $(Na,K)_2CO_3$ and $(Li,Na,K)_2CO_3$; some temperatures are pointed next to the dots.

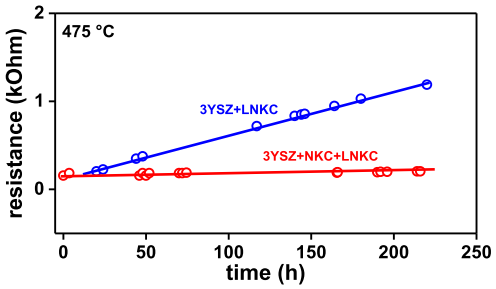

Figure 10. Electrical resistance long-term operational stability data collected at 300 kHz in porous 3YSZ impregnated with $(Li,Na,K)_2CO_3$ and with $(Na,K)_2CO_3$ + $(Li,Na,K)_2CO_3$ at 475 °C.

The resistance values of 3YSZ + LNKC and 3YSZ + NKC + LNKC composite ceramics increase when these samples are kept at a temperature at which the LNKC is in the molten state. That increase is ascribed to reaction of the molten alkali salt with the gold electrode and was evaluated as only 0.4%/day. However, the increase in the resistance of the ceramic composite membrane without the NKC protective layer is more pronounced (5.0%/day), evidence of the action of the NKC protective layer preventing reaction of the molten carbonate with the 3YSZ grain surface. Additional experiments are still required for improving NKC deposition on the porous surface.

3.5. Permeation Measurements. The permeation measurements were performed below 390 °C and above 700 °C, the melting point of the carbonate mixture, using 100 mL min^{-1} flow rate of 50% CO_2 mixed to 50% Ar as the feed gas and N_2 as the sweep gas at the same rate. The following equations evaluate the permeation flux (J) of CO_2 (mL cm^{-2} min^{-1}) through the membrane[10]

$$J_{CO_2\ total} = \frac{P_{CO_2} \cdot f_{gas}}{P_{N_2} \cdot S}$$

$$J_{CO_2\ leak} = \frac{R \cdot P_{Ar} \cdot f_{gas}}{P_{N_2} \cdot S}$$

$$J_{CO_2\ permeated} = J_{CO_2\ total} - J_{CO_2\ leak}$$

R represents the ratio between the concentrations of CO_2 and Ar detected below 500 °C on the permeated side, while S denotes the surface area of the membrane in contact with the feed gas.

https://doi.org/10.1021/acs.energyfuels.3c05216
Energy Fuels 2024, 38, 9890−9897

Considering the active area of the membrane, the permeation flux of the membrane was estimated to be 0.5 mL min^{-1} cm^{-2}. Normalizing by the partial pressure of CO_2 on each side, the permeance of the membrane at 700 °C was estimated to be 8.0 × 10^{-8} mol m^{-2} s^{-1} Pa^{-1}, in agreement with previous results with a gadolinium-doped ceria/lithium−sodium carbonate.[27]

4. CONCLUSIONS

Porous 3YSZ ceramic pellets with high skeletal density were prepared by mixing with PMMA, which was subsequently thermally removed during sintering. The pellets were then subjected to alkali salts' vacuum-assisted impregnation, with the pores filled either with molten eutectic $(Li,Na,K)_2CO_3$ (LNKC) composition or with molten eutectic $(Na,K)_2CO_3$ (NKC) followed by molten LNKC compositions. Electrochemical impedance spectroscopy data were collected at 475 °C, a temperature exceeding the melting point of LNKC. The main results, evaluated by the carbon dioxide ion conductivity of molten LNKC across the porous membrane, show that coating the pore surfaces with NKC hinders the reaction of molten LNKC with the 3YSZ grains, thereby enhancing the membrane's carbon dioxide capture long-time performance. This experimental procedure may be a way for the development of solid state devices for the capture of CO_2, being suggested to be applied to other solid electrolyte/alkali salts membranes.

AUTHOR INFORMATION

Corresponding Author

Reginaldo Muccillo − *Center of Science and Technology of Materials, Energy and Nuclear Research Institute, São Paulo, São Paulo 05508-000, Brazil;* orcid.org/0000-0002-8598-279X; Email: muccillo@usp.br

Authors

Tatiane C. Porfirio − *Center of Science and Technology of Materials, Energy and Nuclear Research Institute, São Paulo, São Paulo 05508-000, Brazil*

Eliana N. S. Muccillo − *Center of Science and Technology of Materials, Energy and Nuclear Research Institute, São Paulo, São Paulo 05508-000, Brazil*

Complete contact information is available at: https://pubs.acs.org/10.1021/acs.energyfuels.3c05216

Funding

The Article Processing Charge for the publication of this research was funded by the Coordination for the Improvement of Higher Education Personnel - CAPES (ROR identifier: 00x0ma614).

Notes

The authors declare no competing financial interest.

ACKNOWLEDGMENTS

This work was supported by CNEN, CINE-Shell (ANP) (FAPESP Proc. 2017/11937-4), CDMF-CEPID (FAPESP Proc. 2013/07296-2), FAPESP 2020/05250-9, and CNPq (Procs. 402966/2021-0, 306894/2023-8, and 305557/2022-0). The authors acknowledge the Laboratory of Microscopy and Microanalyses—IPEN for EDX analyses and Dr. Sabrina G. M. Carvalho for thermal analyses. T.C.P. acknowledges CINE-Shell (ANP) (FAPESP Proc. 2017/11937-4) and Intercentros IPEN 2020.06.IPEN.01 for the postdoctoral fellowships.

REFERENCES

(1) Cassir, M.; Belhomme, C. Technological applications of molten salts: the case of the molten carbonate fuel cell. *Plasmas Ions* **1999**, *2*, 3−15.

(2) Wade, J. L.; Lackner, K. S.; West, A. C. Transport model for a high temperature, mixed conducting CO_2 separation membrane. *Solid State Ionics* **2007**, *178*, 1530−1540.

(3) Li, Y.; Rui, Z.; Xia, C.; Anderson, M.; Lin, Y. S. Performance of ionic-conducting ceramic/carbonate composite material as solid oxide fuel cell electrolyte and CO_2 permeation membrane. *Catal. Today* **2009**, *148*, 303−309.

(4) Rui, Z.; Anderson, M.; Lin, Y. S.; Li, Y. Modeling and analysis of carbon dioxide permeation through ceramic-carbonate dual-phase membranes. *J. Membr. Sci.* **2009**, *345*, 110−118.

(5) Lapa, C. M.; Figueiredo, F. M. L.; de Souza, D. P. F.; Song, L.; Zhu, B.; Marques, F. M. B. Synthesis and characterization of composite electrolytes based on samaria-doped ceria and Na/Li carbonates. *Int. J. Hydrogen Energy* **2010**, *35*, 2953−2957.

(6) Wade, J. L.; Lee, C.; West, A. C.; Lackner, K. S. Composite electrolyte membranes for high temperature CO_2 separation. *J. Membr. Sci.* **2011**, *369*, 20−29.

(7) Dong, X. L.; Ortiz Landeros, J.; Lin, Y. S. An asymmetric tubular ceramic-carbonate dual phase membrane for high temperature CO_2 separation. *Chem. Commun.* **2013**, *49*, 9654−9656.

(8) Marques, F. M. B.; Patrício, S.; Muccillo, E. N. S.; Muccillo, R. On the model performance of composite CO_2 separation membranes. *Electrochim. Acta* **2016**, *210*, 87−95.

(9) Carvalho, S. G. M.; Muccillo, E. N. S.; Marques, F. M. B.; Muccillo, R. Electric field-assisted sintering (gadolinia-doped ceria/alkali salts) composite membranes. *Materialia* **2020**, *11*, 100679.

(10) Carvalho, S. G. M.; Muccillo, E. N. S.; Fonseca, F. C.; Müller, M.; Schulze-Küppers, F.; Baumann, S.; Meulenberg, W. A.; Guillon, O.; Muccillo, R. Tape-casting and freeze-drying gadolinia-doped ceria composite membranes for carbon dioxide permeation. *J. Membr. Sci.* **2022**, *648*, 120355.

(11) Anderson, M.; Lin, Y. S. Carbonate-ceramic dual-phase membrane for carbon dioxide separation. *J. Membr. Sci.* **2010**, *357*, 122−129.

(12) Norton, T. T.; Lu, B.; Lin, Y. S. Carbon dioxide permeation properties and stability of samarium-doped-ceria carbonate dual-phase membranes. *J. Membr. Sci.* **2014**, *467*, 244−252.

(13) Zhang, L.; Li, X.; Wang, S.; Romito, K. G.; Huang, K. High conductivity mixed oxide-ion and carbonate-ion conductors supported by a prefabricated porous solid-oxide matrix. *Electrochem. Commun.* **2011**, *13*, 554−557.

(14) Zhang, L.; Mao, Z.; Thomason, J. D.; Wang, S.; Huang, K. Synthesis of a homogeneously porous solid oxide matrix with tunable porosity and pore size. *J. Am. Ceram. Soc.* **2012**, *95*, 1832−1837.

(15) Patrício, S. G.; Soares, C. M. C.; Santos, C. F. N.; Figueiredo, F. M. L.; Marques, F. M. B. Ceria-based substrates for CO_2 separation membranes. *Solid State Ionics* **2014**, *262*, 248−252.

(16) Patrício, S. G.; Papaioannou, E.; Zhang, G.; Metcalfe, I. S.; Marques, F. M. B. High performance composite CO_2 separation membranes. *J. Membr. Sci.* **2014**, *471*, 211−2018.

(17) Evans, A.; Xing, W.; Norby, T. Electromotive Force (emf) Determination of Transport Numbers for Native and Foreign Ions in Molten Alkali Metal Carbonates. *J. Electrochem. Soc.* **2015**, *162*, F1135−F1143.

(18) Gong, Y.; Li, X.; Zhang, L.; Tharp, W.; Qin, C.; Huang, K. Molten Carbonates as an Effective Oxygen Reduction Catalyst for 550−650°C Solid Oxide Fuel Cells. *J. Electrochem. Soc.* **2013**, *160*, F958−F964.

(19) Milewski, J.; Podhurska, V.; Martsinchyk, A.; Vasyliv, B.; Dybinski, O. Experimental and theoretical investigation of contact resistance in molten carbonate fuel cells. *J. Power Sources* **2023**, *568*, 232952.

(20) Jamale, A.; Starykevich, M.; Marques, F. M. B. Elucidation of subtle degradation mechanisms in composite CO_2 separation membranes. *J. Membr. Sci.* **2022**, *662*, 120968.
(21) Zhao, X.; Zhang, R.; Liu, Y.; He, M.; Su, Y.; Gao, C.; Jiang, Z. Antifouling membrane surface construction: Chemistry plays a critical role. *J. Membr. Sci.* **2018**, *551*, 145−171.
(22) Rana, D.; Matsuura, T. Surface modifications for antifouling membranes. *Chem. Rev.* **2010**, *110*, 2448−2471.
(23) Lemes-Rachadel, P.; Garcia, G. S.; Machado, R. A. F.; Hotza, D.; Costa, J. C. D. d. Current developments of mixed conducting membranes on porous substrates. *Mater. Res.* **2013**, *17*, 242−249.
(24) https://www.tosoh.com/our-products/advanced-materials/zirconia-powders. Accessed: August 08, 2023.
(25) Frangini, S.; Masi, A. Molten carbonates for advanced and sustainable energy applications: Part I. Revisiting molten carbonate properties from a sustainable viewpoint. *Int. J. Hydrogen Energy* **2016**, *41*, 18739−18746.
(26) Muccillo, R.; Kleitz, M.; Muccillo, E. N. Flash grain welding in yttria stabilized zirconia. *J. Eur. Ceram. Soc.* **2011**, *31*, 1517−1521.
(27) Carvalho, S. G. M.; Muccillo, E. N. S.; Muccillo, R. Design and validation of an experimental setup for evaluation of gas permeation in ceramic membranes. *Membranes* **2023**, *13*, 246.
(28) Garvie, R. C. The occurrence of metastable tetragonal zirconia as a crystallite size effect. *J. Phys. Chem.* **1965**, *69*, 1238−1243.
(29) tetragonal phase of 3YSZ: PDF 82-1245; monoclinic phase: PDF 37-1484.
(30) Muccillo, R. Impedance spectroscopy analysis of zirconia:8 mol % yttria solid electrolytes with graphite pore former. *J. Mater. Res.* **2009**, *24*, 1780−1784.
(31) Steil, M. C.; Thevenot, F.; Kleitz, M. Densification of yttria-stabilized zirconia - impedance spectroscopy analysis. *J. Electrochem. Soc.* **1997**, *144*, 390−398.
(32) Savova-Stoynov, B.; Stoynov, Z. B. Analysis of the inductance influence on the measured electrochemical impedance. *J. Appl. Electrochem.* **1987**, *17*, 1150−1158.
(33) Subbarao, E. C. Zirconia - an overview. *Advances in Ceramics, Science and Technology of Zirconia*; The American Ceramic Society, 1981; Vol. *3*; pp 1−25.

https://doi.org/10.1021/acs.energyfuels.3c05216
Energy Fuels 2024, 38, 9890−9897